geoconvention
Calgary • Canada • May 7-11 2018

Understanding shear behaviour of a rough joint using surface topography scan and numerical simulation

Qi Zhao and Giovanni Grasselli

Department of Civil Engineering, University of Toronto, Toronto, ON, Canada. Email: q.zhao@mail.utoronto.ca

Summary

In this study, we combine rotary shear test, surface topography scan, and numerical simulation to investigate shear behaviour of a rough joint. We first registered the joint surfaces with topography scans, then the joint was tested by means of rotary shear. We then built a two-dimensional (2D) model based on the surface topography scan to partially reproduce the experiment results. The simulation results qualitatively captured the realistic emergent rock mechanical and frictional behaviours and suggested that surface geometry (i.e. roughness) controlled the initiation stage of slip.

Introduction

The study of shear behaviour of rough surfaces is essential for understanding induced earthquakes. In laboratory studies, rotary shear experiments are usually used to investigate shear behaviour; for its advantages in unlimited shear distance and constant nominal contact area. We conducted a rotary shear experiment on a rough joint, recording the normal and shear stresses during shearing. Then, a numerical simulation using the hybrid finite-discrete element method (FDEM) was conducted to improve the understanding of the experiment results. This numerical model was generated based on the topography scan of the fresh joint surfaces and configured according to the actual testing conditions. The simulation results provided insights in the time-continuous variation of stresses on the shear surface and suggested the significant influence of surface asperities on slip behaviour.

Theory and/or Method

FDEM is a numerical method that combines continuum mechanics principles with discrete element method to simulate interaction, deformation, and fracturing of materials (Munjiza, 2004). FDEM has the ability to explicitly capture the entire deformation and fracturing process, as well as the associated microseismic events (Mahabadi, 2012; Lisjak, 2013; Zhao, 2015).

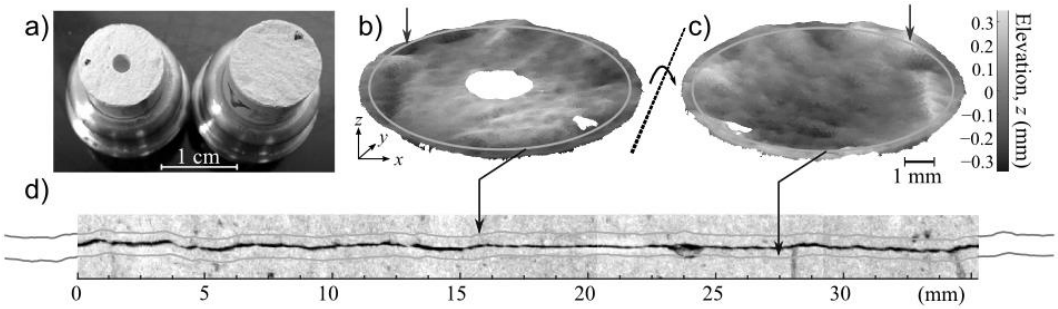

Figure 1. Preparation of 2D surface profiles for the model setup. (a) The top (left) and bottom (right) semi-samples used in the rotary shear experiment. (b)–(c) 3D surface scan of joint surfaces. Arrows show the location with the largest surface amplitude. (d) Comparison of the extracted profiles with the micro-CT image showing the initial condition of the shear simulation. The profiles were vertically offset for clearer illustration.

We built the model honouring the sample geometry and test conditions. The sample assembly consisted of the top and bottom semi-samples, with the rough joint surfaces between them that were created via a three-point bending (Figure 1a). However, due to the limitation of the 2D simulation, the geometry of the fault could not be directly modelled. Instead, the surfaces were first scanned using a 3D surface scanner (ATOS II by GOM), and then the circular profiles corresponding to the largest roughness (i.e., highest asperity) on the surfaces were extracted (Figure 1b and c). The positions of these profiles were adjusted to match the initial contact condition of the experiment, which was imaged by X-ray micro-CT (Figure 1d). Finally, the FDEM model was established using these adjusted profiles with a graded mesh to reduced the computational demand (Figure 2).

The boundary conditions were applied according to the experiment. The simulation of the shear test was conducted in three phases: (1) applying the initial normal stress of 2.5 MPa, (2) damping out vertical oscillation and ramping up shear velocity, and (3) applying shear displacement. Moreover, numerical material properties (e.g., elastic modulus, fracture energy, strength, etc.) were calibrated according to laboratory tests (i.e., unconfined/confined compression tests and Brazilian disc tests) to ensure the simulated material could correctly reproduce the emergent material properties of the sample (Zhao, 2017).

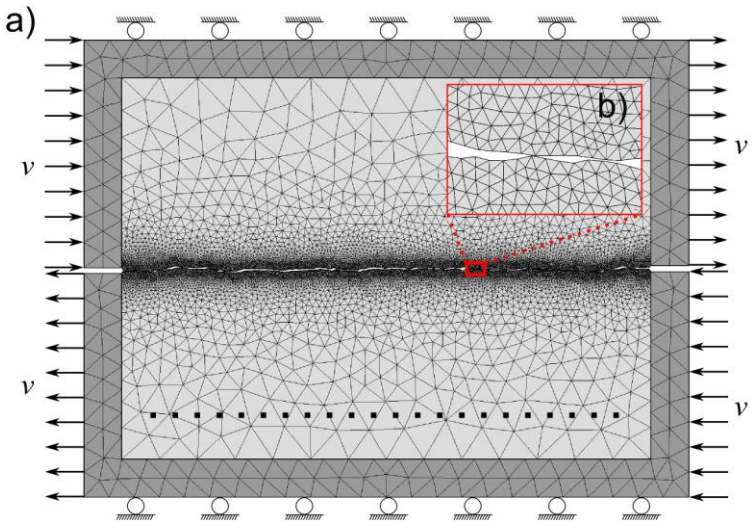

Figure 2. (a) Mesh topology and boundary conditions of the simulation. The joint was first loaded in the normal direction to 2.5 MPa, and then the vertical positions of the shear boxes were fixed by rollers, and shear velocity was applied as indicated by the arrows. The dotted line shows the location of the virtual measurement line, and the apparent shear and normal stresses were calculated by averaging the corresponding values of the elements on the measurement line. (b) Zoom-in view of the refined mesh at the joint surface.

Results

The shear stress (τ) and normal stress (σ_n) were recorded for both the experiment and the simulation and used to calculate the friction coefficient (μ). Simulated stresses suffered significant fluctuations, resulting in large oscillations in the calculated μ. On the other hand, the simulated μ was much lower than the experimental measurement, which is due to the limitation of 2D simulation that could not capture the particle motions in the third dimension. Nonetheless, appealing similarities were observed between the experiment and simulation results.

The initial portion of the simulated shear behaviour qualitatively resembled the laboratory test results (Figure 3). Four stages of behaviour can be clearly identified in both data sets, and this observation suggests that the 2D profile that we used in the simulation, with the highest roughness on the surface, may have controlled the initial portion of slip behaviour.

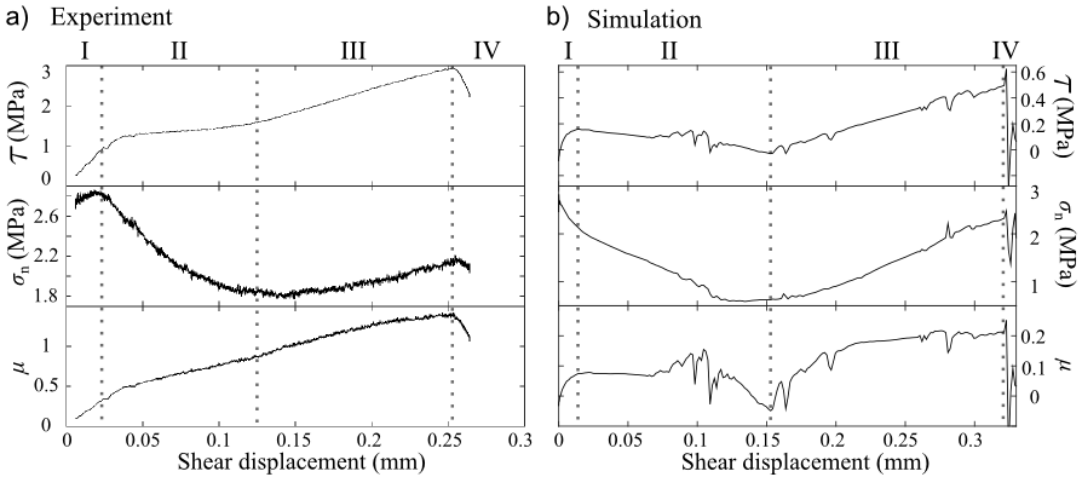

Figure 3. Comparison of stresses and friction coefficient of the initial portion of slipping between (a) the laboratory data and (b) the simulated data.

To further understand what caused the distinguished behaviour in these four stages, we took a closer look at the stress conditions and mechanical interaction of the asperity that was associated with the significant stress drop at stage IV (Figure 4).

This detailed observation provided us the time-continuous stress variation on the fault surface, allowing us to explain the laboratory observations and achieve better comprehension of how the interaction between asperities controlled the frictional behaviour. In particular:

I. During stage I, the shear stress increased gradually due to frictional resistance of the contact points under normal stress. Note that the minor normal stress increase measured in the experiment at this stage was not captured by the numerical model. This may be related to the interaction of the asperities in the direction perpendicular to shear (i.e., out-of-plane motion), which was not captured by the simulation.

II. During stage II, the top and bottom surfaces adjusted to a more conforming contact, which resulted in a decrease of the normal stress at the asperity contact. The asperities rarely interacted at this stage; therefore, the shear stress did not increase with the increasing shear displacement.

III. During stage III, the contact points shifted and asperities started to engage and interlock, causing the shear stress to increase quickly and reach the peak shear stress at the end of this stage. The asperities stayed intact and “climbed” onto each other, causing dilation and increased the normal stress.

IV. At the beginning of stage IV, the asperity under high stress concentration broke and released the accumulated normal and shear strain locally, resulting in the drop of shear and normal stresses.

Conclusions

Taking advantage of surface topography and FDEM numerical simulation, we partially reproduced a rotary shear experiment. The model captured the mechanical and frictional behaviours observed in the laboratory experiment, providing detailed information of the continuous variation of stresses on the shear surface. The model suggested the importance of fault surface geometry in controlling joint slip, and we were able to explain the laboratory observations with the help of these results. This study demonstrated that micromechanical based numerical simulation is a capable approach to study joint slip behaviour.

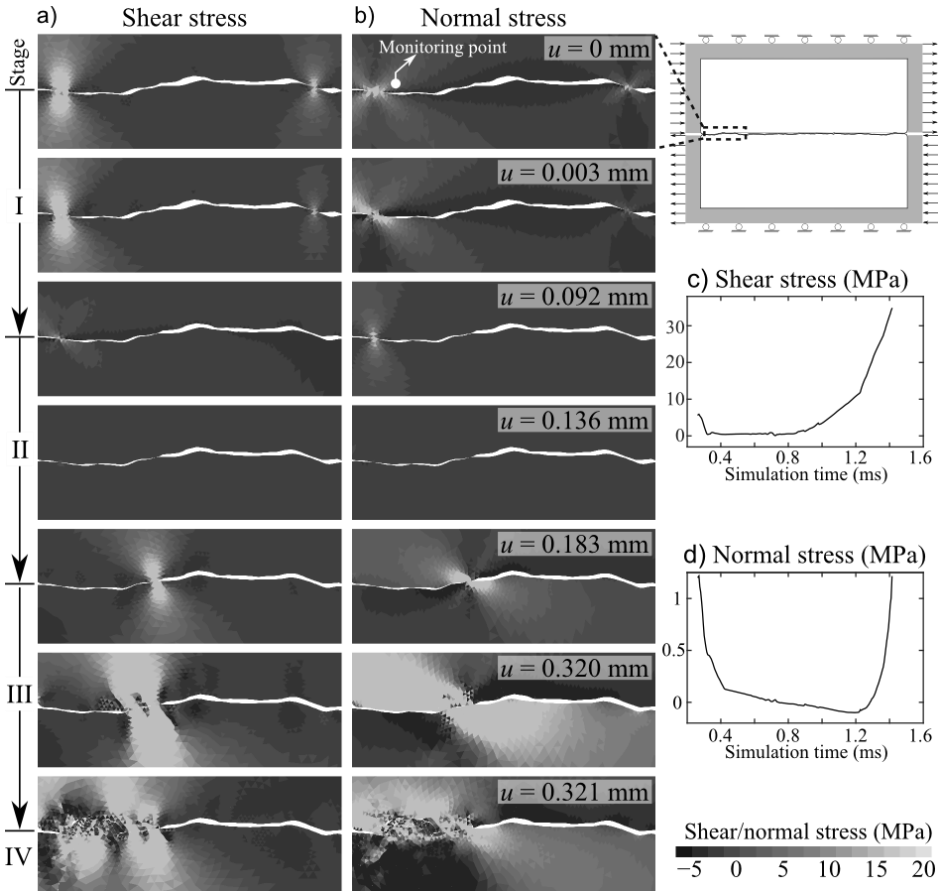

Figure 4. Detailed stress conditions near the joint surface at stages I–IV. Local shear stress (panel a) and normal stress (panel b) are illustrated at different shear displacement (*u*). (c) and (d) are the shear and normal stress conditions at the monitoring point, respectively. Note that negative stress indicates compression.

Acknowledgements

This work has been supported through the NSERC Discovery Grants 341275, CFI-LOF Grant 18285, Carbon Management Canada (CMC), and Foundation CMG Research Chair program. The authors would like to thank Geomechanica Inc. for providing the Irazu FDEM simulation software.

References

Munjiza, A. (2004) The Combined Finite-Discrete Element Method. John Wiley & Sons, Ltd.

Mahabadi, O. K., Lisjak, A., Munjiza, A. and G. Grasselli. (2012) Y-Geo: New Combined Finite-Discrete Element Numerical Code for Geomechanical Applications. International Journal of Geomechanics, 12(6):676–688.

Lisjak, A., Liu, Q., Zhao, Q., Mahabadi, O. K. and G. Grasselli. (2013) Numerical simulation of acoustic emission in brittle rocks by two-dimensional finite-discrete element analysis. Geophysical Journal International, 195(1):423–443.

Zhao, Q., Tisato, N., Grasselli, G., Mahabadi, O. K., Lisjak, A. and Q. Liu. (2015) Influence of in situ stress variations on acoustic emissions: a numerical study. Geophysical Journal International, 203(2):1246–1252.

Zhao, Q. (2017) Investigating brittle rock failure and associated seismicity using laboratory experiments and numerical simulations. PhD thesis, University of Toronto.